Fibers and Polymers 2016, Vol.17, No.2, 174-180
DOI 10.1007/s12221-016-5827-y

ISSN 1229-9197 (print version)
ISSN 1875-0052 (electronic version)

Functionalization of Graphene Nanosheets and Its Dispersion in PMMA/PEO Blend: Thermal, Electrical, Morphological and Rheological Analyses

Elham Aram[1], Morteza Ehsani[1]*, Hossein Ali Khonakdar[1,2], Seyed Hassan Jafari[3], and Nastaran Riahi Nouri[4]

[1]*Iran Polymer and Petrochemical Institute, Tehran 14965-115, Iran*
[2]*Leibniz Institute of Polymer Research, Dresden D-01067, Germany*
[3]*School of Chemical Engineering, University of Tehran, Tehran 11155-4563, Iran*
[4]*Niroo Research Institute, Ceramic & Polymer Group, Tehran 14665-517, Iran*
(Received November 9, 2015; Revised January 12, 2016; Accepted January 15, 2016)

Abstract: Graphene nanoplatelet (GnP) was chemically functionalized by amine groups for improvement of compatibility in poly(methyl methacrylate) (PMMA)/poly(ethylene oxide) (PEO) blend. PMMA/PEO (90/10) nanocomposites with non-functionalized GnP and functionalized GnP (FGnP) were prepared by solution casting method. Successful grafting of amine groups on the GnP surface was confirmed by Fourier transform infrared (FT-IR) and X-ray diffraction (XRD) analysis. The Transmission electron microscopy (TEM) images showed that the dispersion state of FGnP was better than that of GnP in PMMA/PEO nanocomposites. The effects of FGnP and GnP on rheological, thermal and electrical properties of PMMA/PEO nanocomposites were investigated by various methods. The results indicated that the FGnP-based nanocomposites had higher storage modulus, glass transition temperature and thermal stability as compared to the GnP-based nanocomposites. The electrical conductivity of the nanocomposites with FGnP was better than that of GnP-based nanocomposites. The higher conductivity was attributed to homogeneous and well dispersion state of FGnP in PMMA/PEO nanocomposites.

Keywords: Graphene, Para-phenylene diamine, Poly(methyl methacrylate)/poly(ethylene oxide), Nanocomposites, Dispersion of GnP

Introduction

In recent years, there has been a vast interest towards polymer blending because of its economical advantages and producing new polymeric materials with improved properties [1,2]. Among different blends, poly(methyl methacrylate)/ poly(ethylene oxide), (PMMA/PEO), blend has a large share in the plastics and composites applications due to its excellent processability and optical properties [3-5]. However, some properties of PMMA/PEO blend such as electrical, thermal and mechanical properties need to be improved to meet the requirements of further applications. Carbon based materials such as graphite powder, carbon black, graphene nanoplatelet and carbon nanotube are suitable candidates to improve the final properties of homopolymers [6-8]. Among these, graphene nanoplatelet (GnP) having nanometer thickness and diameter in micrometer scale has recently attracted enormous attention due to its excellent electrical conductivity, high thermal conductivity, superior mechanical properties and very high surface area [9-11]. However, graphene is a new class of one atom thick, two-dimensional sheet of sp^2-hybridized carbon atoms that are closely packed in a honeycomb structure. Because of extraordinary physical, chemical, and mechanical properties [12-15], the graphene nanoplatelets have been widely applied in many fields such as polymer composites, molecular sensors, drug delivery, supercapacitors, gas storage materials and nanoelectronic devices [16-19]. However, the physicochemical properties of polymer nanocomposites depend on the dispersion of graphene in polymer matrices and proper interfacial bonding between polymer and graphene. Graphene nanoplatelets tend to agglomerate during the preparation of the nanocomposites due to their large specific surface area and the strong attractive van der Waals forces between the platelets, which lowers the effect of graphene reinforcement on polymer properties [14,20]. Several methods have been developed for efficient dispersion of graphene in polymer matrices, including surface modification, wrapping, electrospinning, and use of surfactants [21-24]. Surface modification and functionalization of graphene is an effective method to prevent the agglomeration and enhance the interaction between graphene nanoplatelet and polymer matrix [21]. In view of this, Zhang *et al.* functionalized graphene oxide (GO) with diisocyanates to prevent aggregation of the nanosheets [25]. Wenjuan *et al*. [26] have reported that functionalization of GO with octadecylamine can improve its dispersion in polystyrene (PS). The functionalized graphene increased electrical conductivity of PS. In another study, GO was functionalized based on the reaction of ethylene diamine with epoxy groups of the GO nanosheets, which effectively decreased face-to-face stacking of the nanosheets [27].

The aim of this work is to functionalize graphene nanoplatelets with para-phenylene diamine (PPD) by a nucleophilic ring opening reaction and to study dispersion state of the functionalized graphene nanoplatelete (FGnP) in PMMA/ PEO blend. The effect of FGnP and pristine GnP on various

*Corresponding author: M.Ehsani@ippi.ac.ir

properties of the developed nanocomposites will be explored through morphological, electrical, rheological and thermal properties analyses.

Experimental

Materials

Poly(methyl methacrylate) (PMMA) (M_w=1.2×10^5 g/mol), poly(ethylene oxide) (PEO) (M_w=1×10^5 g/mol) were purchased from Sigma-Aldrich. These materials were dried at 50 °C in a vacuum oven for 24 h. Potassium permanganate ($KMnO_4$), sodium nitrate ($NaNO_3$), hydrogen peroxide (H_2O_2, 30 %) and hydrochloric acid (HCl, 37 %) were supplied by Sigma-Aldrich. GnP grade C-750 with an average diameter of 2 μm and surface area of 750 m^2/gr was obtained from XG Sciences (USA) and was dried in a complete vacuum at 80 °C for 24 h. As received, the particles often agglomerate and form large powders. Para-phenylene diamine, N,N-dimethyl formamide, concentrated sulphuric acid (H_2SO_4 95-98 %), ethanol (99.7 %) and ammonia (NH_3) were purchased from Merck chemical company.

Chemical Functionalization of GnP

Graphene nanoplatelets were oxidized by the modified Hummers method [28]. In brief, 1 g of GnP, 0.5 g of $NaNO_3$ and 30 m*l* of H_2SO_4 were mixed in an ice bath. Subsequently, 3 g of $KMnO_4$ was slowly added. The ice bath was removed and the resulting mixture was stirred for 5 h at room temperature. Then, 46 m*l* of deionized water was added and the mixture was refluxed for 30 min. The reaction was terminated by addition of hot deionized water and 30 % hydrogen peroxide. The product was washed with a solution of 10 % HCl and deionized water until it reached to a pH of about 7, then dried in a vacuum oven at 80 °C before use.

For the preparation of FGnP, 0.5 g of oxidized GnP was ultrasonically dispersed in 400 m*l* deionized water for 1 h. Subsequently, the mixture was reacted with a solution of water and PPD (3 g) in the presence of NH_3 at 90 °C overnight. The resulting mixture was filtrated with a PP membrane, thoroughly washed with a 1:1 ethanol-water mixture for several times. Finally, FGnP was obtained by drying in a vacuum oven at 80 °C for 24 h.

Preparation of PMMA/PEO Nanocomposites

Various PMMA/PEO/GnP, PMMA/PEO/FGnP nanocomposites were prepared via solution casting using N,N-dimethyl formamide as the solvent. Desired amounts of GnP were dispersed in N,N-dimethyl formamide by ultrasonication for 2 h and sonicated for 5 min to yield a homogeneous dispersion. A certain amount of PMMA/PEO (90/10) was dissolved in N,N-dimethyl formamide under stirring at 50 °C until a homogenous solution has been formed. Then, PMMA/PEO solution was gradually added to GnP dispersion and stirred for 5 h at 50 °C to obtain a fine dispersion assisted by gradual evaporation of the solvent. Finally, the composite solution was poured into a glass petri dish and dried at room temperature for 24 h. For complete removal of the solvent, the samples were vacuum dried at 50 °C for 2 days. Due to hygroscopic nature of PEO, all the casting and drying processes were done in a glove box under nitrogen blanket. PMMA/PEO/FGnP composites were prepared by the same procedure. These nanocomposites were compression molded to 1 mm thick plates by a hot press at 140 °C.

In order to better show the difference between the influence of GnP and FGnP on polymer properties, the graphene content of 0.5, 1 and 10 wt% were selected to compare the properties of PMMA/PEO/FGnP with PMMA/PEO/GnP nanocomposites. The samples have been designated as neat PMMA/PEO, PMMA/PEO/GnP-0.5, PMMA/PEO/GnP-1, PMMA/PEO/GnP-10, PMMA/PEO/FGnP-0.5, PMMA/PEO/FGnP-1 and PMMA/PEO/FGnP-10 where the numbers show the weight fraction of incorporated nanofillers.

Characterization Techniques

Fourier transform infrared (FT-IR) measurements were carried out to characterize functional groups of GnP and FGnP by using a Bruker-IFS-48 FT-IR spectrometer (Ettlingen, Germany) in the range of 400-4000 cm^{-1}. X-ray diffraction (XRD) patterns of GnP, oxidized GnP and FGnP were observed on a Simens D 5000 (Germany) X-ray diffractometer with CuK_α radiation operating at 40 Kv and 40 mA. The scanning rate was 4 ° min^{-1} under the diffraction angle, 2θ, in the range of 5-40 °. Transmission electron microscopy (TEM) was carried out with a CM30 (Philips, Holand) at 200 kV to observe the dispersion state of graphene nanosheets within polymer matrix. Rheology measurements were carried out on oscillatory rheometer MCR 300 (Paar Physica) at 140 °C under N_2 atmosphere. The samples were tested on parallel plate geometry with a diameter of 25 mm and a gap size of 1 mm. Dynamic frequency sweep tests were done at frequency range of 0.1-400 rad/s with a constant strain of 10 %, which was within the linear viscoelastic range. The bulk resistivity of the neat PMMA/PEO and its nanocomposites with conductivity lower than 1×10^{-7} S/cm was measured by two-point probe (Keithley 8009 resistivity meter, USA) whereas for materials with conductivity higher than 1×10^{-7} S/cm, the measurement was carried out by a four-point probe (Keithley multimeter DMM2000, USA) with a distance of 16 mm between the inner electrodes and 10 mm between outer electrodes at ambient conditions. The electrical conductivity (σ) of the samples was calculated from the following equation:

$$\sigma(\text{S/cm}) = 1/\rho$$

where ρ is the bulk resistivity of samples. The samples were cut into 0.5 cm×2 cm piece with a thickness of 1 mm. Three samples were used for each measurement and the average values were reported. Differential scanning calorimetry

(DSC) for measurement of glass transition temperature (T_g) was carried out on a Stanton Redcraft STA-780 (London, UK). The samples were heated from -60 to 130 °C with a heating rate of 5 °C/min under nitrogen atmosphere. Thermal stability of nanocomposites was studied by thermogravimetry analysis (TGA) Q500 V6.7 Build 203 instrument. The measurements were carried out from room temperature to 600 °C at a heating rate of 5 °C/min under nitrogen atmosphere.

Results and Discussion

Characterization of Graphene Nanoplatelets

FT-IR Spectra

The FT-IR spectra of GnP, oxidized GnP and FGnP are shown in Figure 1. Before functionalization, GnP shows only an absorption band around 1625 cm^{-1}, which is derived from C=C in aromatic ring, because it has no other specific functional groups on the surfaces. The characteristic peaks due to generated functional groups are appeared in the FT-IR spectrum of oxidized and amine treated GnP. The typical bands of oxidized GnP detected at 1711, 1060, and 1641 cm^{-1} are associated to C=O in carboxyl group, C-O-C in epoxide, and C=C in aromatic ring, respectively [26,27]. Also, a wide band 3000-3500 cm^{-1} is related to O-H band in C-OH groups. FGnP shows new absorption peaks at 1586 cm^{-1} (N-H stretching vibration), 1169 cm^{-1} (C-N stretching vibration) and 723 cm^{-1} (deformation of N-H in -C-NH_2 groups) due to the formation of C-NH-C bands. The intensity of the epoxy band at 1030-1160 cm^{-1} is weakened compared to spectrum of oxidized GnP. The FT-IR results indicate that the amine functional group is grafted on to the surface of GnP by nucleophilic substitution between -NH_2 group of PPD and epoxide group of oxidized GnP.

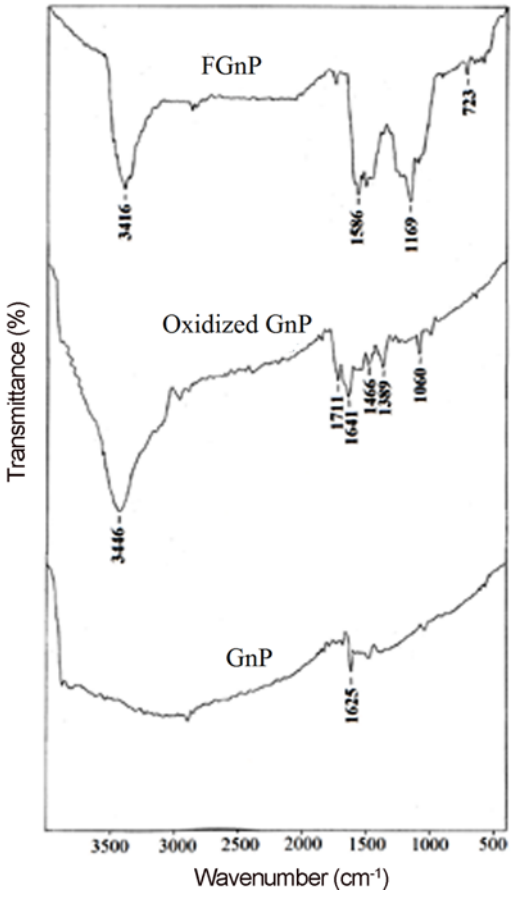

Figure 1. FTIR spectra of GnP, oxidized GnP and FGnP.

X-ray Diffraction (XRD)

XRD measurements were utilized to analyze the structure of layered materials such as graphene nanoplatelets and interlayer spacing between the diffraction planes. The XRD diffraction patterns of GnP, oxidized GnP and FGnP were compared in Figure 2. The characteristic diffraction peak of GnP appeared at 25.64 ° corresponding to an interlayer spacing of about 0.336 nm, which is very close to the d-spacing of graphite [29-31]. By oxidation of GnP, the diffraction peak shifts to 14.32 ° which corresponds to a d-spacing of 0.62 nm. Functionalization of the oxidized GnP with PPD shifts the diffraction angle to 2θ=9.72 ° corresponding to interlayer distance of 0.91 nm and reduces its intensity. This shows that the chemical grafting of PPD onto the oxidized GnP by nucleophilic ring opening reaction leads to a significant enlargement in the interlayer spacing compared to neat GnP. The reduction of the peak intensity may be attributed to the decrease of the crystalline structure of GnP by PPD molecules grafted to the GnP. From this observation, it can be understood that the layered structure of GnP is intercalated by surface functionalization using para-phenylene diamine.

Characterization of Nanocomposites

Morphological Analysis

In order to compare the dispersion state of the graphene nanoplatelets in the matrix, the nanocomposites were investigated by TEM technique. Figure 3(a,b) presents TEM

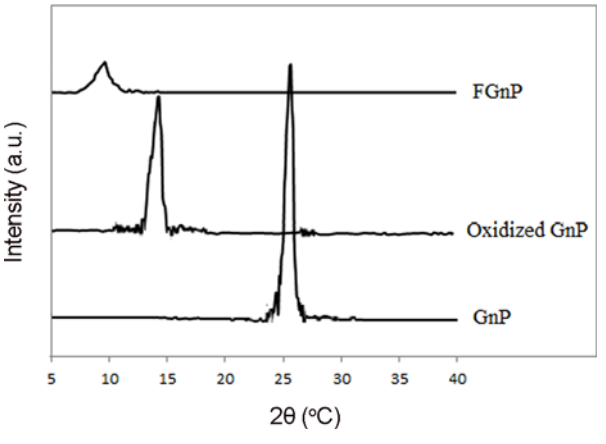

Figure 2. XRD patterns of GnP, oxidized GnP and FGnP.

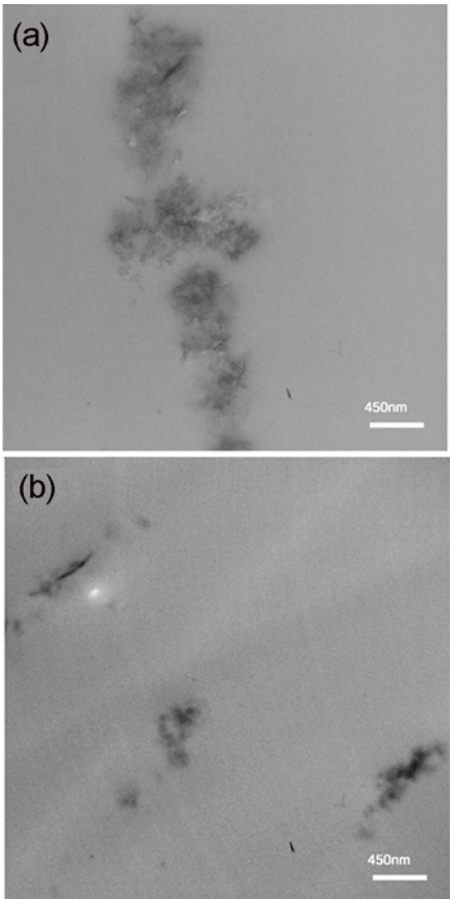

Figure 3. TEM images of (a) PMMA/PEO/GnP-1 and (b) PMMA/PEO/FGnP-1 nanocomposites.

images of PMMA/PEO/GnP-1 and PMMA/PEO/FGnP-1. As can be seen in Figure 3(a,b), FGnP is dispersed more homogeneously in the PMMA/PEO matrix as compared to GnP. This is mainly related to the strong interaction between functional groups of FGnP and matrix and better compatibility between the PMMA/PEO matrix and graphene nanosheets. This phenomenon was also reported elsewhere [32-34].

Rheological Properties

Figure 4 shows the frequency (ω) dependence of the storage modulus (G') and complex viscosity (η^*) of neat PMMA/PEO and its nanocomposites. The storage modulus and complex viscosity of nanocomposites are larger than those of neat PMMA/PEO especially at low frequency regime.

As observed from Table 1, the slope of the G' curves decreases with the addition of graphene to the PMMA/PEO. As previously reported [18-22], the increase of the storage modulus, complex viscosity and the decrease of the slope of storage modulus curves, especially at low frequencies are closely related to the incorporation of filler and its dispersion state in polymer matrix. In this study, the strong polymer-graphene and graphene-graphene interactions may lead to interconnection of the graphene nanoplatelets and formation

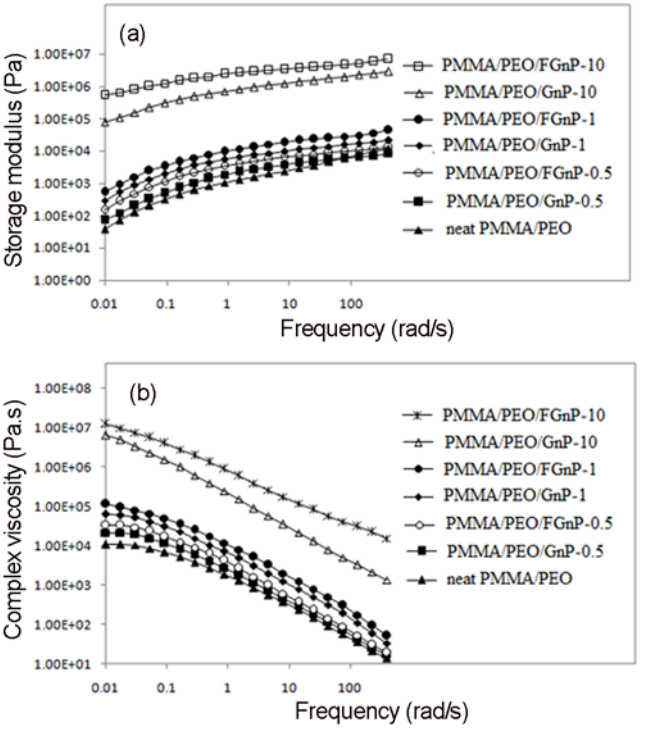

Figure 4. Rheological properties of neat PMMA/PEO and its nanocomposites; (a) storage modulus (G') and (b) complex viscosity (η^*).

Table 1. Slope of the (G') curves for the neat PMMA/PEO and the nanocomposites

Sample	Slope of the (G') curves
Neat PMMA/PEO	1.12
PMMA/PEO/GnP-0.5	0.932
PMMA/PEO/GnP-1	0.825
PMMA/PEO/GnP-10	0.598
PMMA/PEO/FGnP-0.5	0.864
PMMA/PEO/FGnP-1	0.743
PMMA/PEO/FGnP-10	0.379

of a network-like structure, which can effectively restrict chain motion and cause a solid-like rheological behavior [35,36]. The results show that FGnP-based nanocomposites have higher storage modulus and lower slope of storage modulus curves than GnP-based nanocomposites at the same concentration of filler, because the interfacial bonding between the graphene and the polymer matrix increases and the dispersion is improved when the GnP surface is modified. As a result, better dispersion of graphene particles leads to more complete formation of graphene network structure, which can cause more limitation of the polymer chains motion and a more solid-like rheological behavior. Also, reduced mobility of the polymer chains due to interaction

matrix molecules with filler and finer dispersion of FGnP may be the source of the η^* increase [32,37]. It is notable from Figure 4 and Table 1 that the further addition of graphene concentration into polymer matrix increases the storage module, complex viscosity and decreases the slope of storage module curves. Therefore, the rheological results confirm that the modified graphene nanoplatelets have better dispersion state in PMMA/PEO matrix as compared to GnP due to functionalization.

Electrical Conductivity

It is well known that intrinsic electrical conductivity, concentration, aspect ratio, surface treatment and dispersion state of graphene in polymer affect the electrical properties of polymer composites [38]. Figure 5 presents the effect of surface modification of GnP on the electrical conductivity of PMMA/PEO. As is seen, both GnP and FGnP effectively increase the electrical conductivity of neat PMMA/PEO blend by forming conducting networks of the graphene nanosheets in composites. As graphene loading is increased, the electrical conductivity of PMMA/PEO is further increased. The enhancement of the electrical conductivity in the PMMA/PEO/FGnP based nanocomposites is stronger than PMMA/PEO/GnP based nanocomposites. For instance, the incorporation of 10 wt% GnP and FGnP increases the electrical conductivity by about 11 and 12 orders of magnitude, respectively. In general, the grafted para-phenylene diamine groups on GnP can form hydrogen bonding with matrix, improve the interfacial adhesion between graphene and PMMA/PEO blend as well as the dispersion of nanoplatelets in polymer matrix. This can result in production of additional electrical pathways and ease of interconnected network structure formation. However, GnP is less effective in increasing the electrical conductivity of PMMA/PEO due to its poor dispersion, although it has a higher intrinsic electrical conductivity in comparison with FGnP. Similar results were reported in PMMA/graphite and PEO/graphene composites

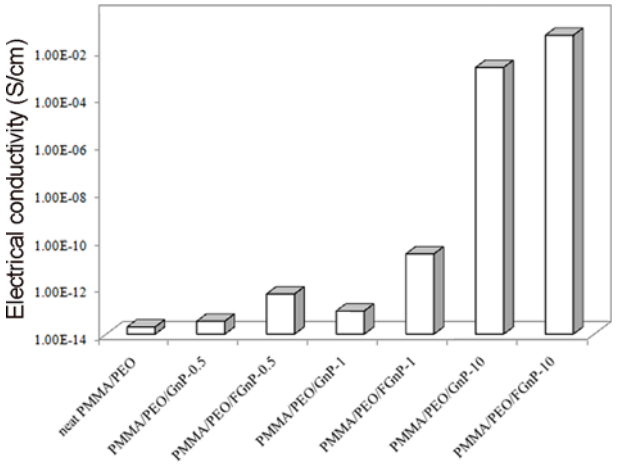

Figure 5. Electrical conductivity of neat PMMA/PEO and its nanocomposites.

Table 2. T_g values of the neat PMMA/PEO and its nanocomposites

Sample	T_g (°C)
Neat PMMA/PEO	94.5
PMMA/PEO/GnP-0.5	98
PMMA/PEO/GnP-1	102
PMMA/PEO/GnP-10	106.5
PMMA/PEO/FGnP-0.5	103
PMMA/PEO/FGnP-1	108.6
PMMA/PEO/FGnP-10	114.9

[39,40]. Therefore, surface treatment of GnP with PPD can improve homogeneous dispersion of nanosheets in polymer leading to a better enhancement in the electrical conductivity of PMMA/PEO blend.

DSC Analysis

Glass transition temperature (T_g) of the neat PMMA/PEO and its nanocomposites were determined using DSC analysis and the results are summarized in Table 2. The temperature corresponding to the middle point of the temperature range in which the specific heat capacity jumps from the value of glassy state to that of rubbery state is considered as T_g by DSC analysis. Compared to that of neat PMMA/PEO, nanocomposites with GnP exhibit 7.5 and 12 °C increase in T_g whereas nanocomposites with FGnP show 14.1 and 20.4 °C increase in T_g at 1 and 10 wt% of nanofiller loadings, respectively. The improvement in the T_g of these nanocomposites is related to reduction of the chain movement due to the interaction between the polymer chains and 2D-layered graphene incorporated, which is similar to findings reported by other researchers [32,37]. Further increase of T_g of FGnP-based nanocomposites as compared to GnP-based nanocomposites is due to stronger interaction between the functional groups of FGnP and matrix, which consequently results in a better adhesion. In addition, FGnP acting as larger obstacles, causes stronger mechanical interlockings between the graphene nanosheets and the polymer chains, which can prevent the polymer molecules to rotate and slip, so a higher T_g is shown.

TGA Analysis

Thermogravimetric profiles of the neat PMMA/PEO and its nanocomposites containing 1 and 10 wt% of the GnP and FGnP are presented in Figure 6. According to the curves, all the samples are decomposed in two steps. The first and second stages of decomposition are due to the monomer evolution initiated at unsaturated chain ends and degradation of PEO and PMMA, respectively [41]. It is notable that all samples exhibit small weight loss at the first step. Nanocomposites exhibit higher thermal stability than the neat PMMA/PEO due to the incorporation of graphene. It was reported that graphene layers act as physical barriers and

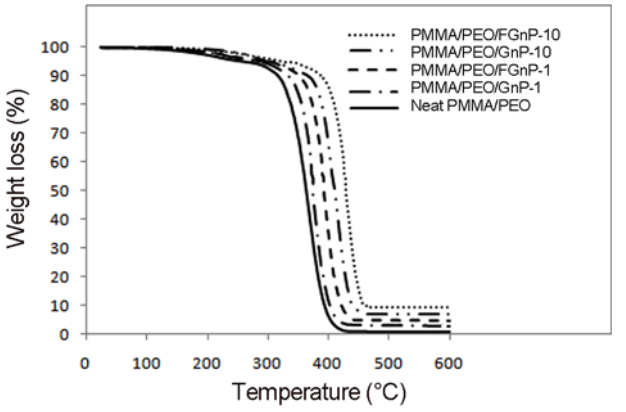

Figure 6. TGA thermograms for neat PMMA/PEO, PMMA/PEO/GnP-1, PMMA/PEO/GnP-10, PMMA/PEO/FGnP-1 and PMMA/PEO/FGnP-10 nanocomposites.

could prevent the emission of thermally decomposed small gaseous molecules [42,43]. Results showed that PMMA/PEO nanocomposites exhibited a noticeable increase in thermal stability with increasing of graphene loadings. This indicates that the graphene nanosheets have positive effects on the thermal stability of the nanocomposites. As can be seen, TGA thermogram of PMMA/PEO/FGnP nanocomposite is shifted toward higher temperature and all the degradation temperatures of this nanocomposite are improved significantly as compared to PMMA/PEO/GnP. This is presumably due to homogeneous dispersion of graphenes and stronger interaction between PMMA/PEO matrix and functionalized GnP. Thus, it can be concluded that the FGnP can more effectively prevent the volatilization of organic matrix and hence enhance the thermal stability of composite. Moreover, the char residue contents at the final step in neat PMMA/PEO, PMMA/PEO/GnP-1, PMMA/PEO/FGnP-1, PMMA/PEO/GnP-10 and PMMA/PEO/FGnP-10 are 0.6, 2.69, 4.54, 6.91 and 9.52 wt% respectively. It looks that the better dispersion of graphenes leads to higher char formation due to high inhibition effect of graphenes on thermal degradation of the PMMA/PEO chains.

Conclusion

PMMA/PEO composites filled with GnP and amine treated GnP were successfully prepared by solvent casting. FT-IR and XRD spectra revealed that functional groups are formed on GnP through chemical functionalization with para-phenylene diamine. TEM images revealed that the FGnP is dispersed more homogeneously throughout the PMMA/PEO matrix as compared to GnP. Rheological characteristics i.e. storage modulus and complex viscosity of FGnP-based nanocomposites were higher than those of GnP-based composites due to strong interaction between FGnP and matrix, which is indicative of better distribution of the graphenes in nanocomposites. Electrical conductivity of FGnP-based nanocomposites was higher than GnP-based nanocomposites due to FGnP improved dispersion and its ease of conducting networks formation. The incorporation of graphenes in PMMA/PEO matrix significantly increased the glass transition temperature and thermal stability of polymer. It should be noted that the homogeneously dispersed graphene layers can prevent the emission of thermally decomposed gaseous molecules, and hence, leading to further enhanced thermal stability of FGnP nanocomposites as compared to GnP nanocomposites. Therefore, these results imply that surface modification of graphene nanoplatelets can improve the dispersion of GnP and leads to better final properties of polymer nanocomposites.

Acknowledgment

The authors would like to acknowledge the Iranian Nanotechnology Initiative (INI) for partial support of this research.

References

1. J. A. Pathak, R. H. Colby, S. Y. Kamath, S. K. Kumar, and R. Stadler, *Macromolecules*, **31**, 8988 (1998).
2. M. Brodeck, F. Alvarez, J. Colmenero, and D. Richter, *Macromolecules*, **45**, 536 (2012).
3. H. B. Kim, J. S. Choi, C. H. Lee, S. T. Lim, M. S. Jhon, and H. J. Choi, *Eur. Polym. J.*, **41**, 679 (2005).
4. K. Jeddi, N. Taheri Qazvini, S. H. Jafari, H. A. Khonakdar, J. Seyfi, and U. Reuter, *J. Polym. Sci. Pt. B-Polym. Phys.*, **49**, 318 (2011).
5. Z. Osman, N. M. Ansor, K. W. Chew, and N. Kamarulzaman, *Ionics*, **11**, 431 (2005).
6. D. H. Yi, H. J. Yoo, and J. W. Cho, *Fiber. Polym.*, **16**, 1766 (2015).
7. B. Qi, Z. Yuan, S. Lu, K. Liu, S. Li, L. Yang, and J. Yu, *Fiber. Polym.*, **15**, 326 (2014).
8. E. Lee and Y. G. Jeong, *Fiber. Polym.*, **16**, 2021 (2015).
9. J. K. Park, I. Do, P. Askeland, and L. T. Drzal, *Compos. Sci. Technol.*, **68**, 1734 (2008).
10. S. Kim, J. Seo, and L. T. Drzal, *Compos. Pt. A-Appl. Sci. Manuf.*, **41**, 581 (2010).
11. K. Kalaitzidou, H. Fukushima, and L. T. Drzal, *Compos. Pt. A-Appl. Sci. Manuf.*, **37**, 1675 (2007).
12. J. W. Jang, B. G. Min, J. H. Yeum, and Y. G. Jeong, *Fiber. Polym.*, **14**, 1332 (2013).
13 Y. Wang, M. Tian, L. Qu, S. Zhu, Y. Sun, and G. Han, *Fiber. Polym.*, **16**, 2011 (2014).
14. Y. Zhu, S. Murali, W. Cai, X. Li, J. W. Suk, J. R. Potts, and R. S. Ruoff, *Adv. Mater.*, **22**, 3906 (2010).
15. M. J. Allen, V. C. Tung, and R. B. Kaner, *Chem. Rev.*, **110**, 132 (2010).
16. J. Wu, W. Pisula, and K. Müllen, *Chem. Rev.*, **107**, 718

(2007).
17. J. E. An, G. W. Jeon, and Y. G. Jeong, *Fiber. Polym.*, **13**, 507 (2012).
18. Y. Shao, J. Wang, H. Wu, J. Liu, I. A. Aksay, and Y. Lin, *Electroanal.,* **22**, 1027 (2010).
19. Y. Zhu, S. Murali, M. D. Stoller, K. J. Ganesh, W. Cai, P. J. Ferreira, A. Pirkle, R. M. Wallace, K. A. Cychosz, M. Thommes, D. Su, E. A. Stach, and R. S. Ruoff, *Science,* **332**, 1537 (2011).
20. K. P. Loh, Q. Bao, P. K. Ang, and J. Yang, *J. Mater. Chem.,* **20**, 2277 (2010).
21. H. Norazlina and Y. Kamal, *Polym. Bull.,* **72**, 931 (2015).
22. V. H. Pham, T. V. Cuong, T. T. Dang, S. H. Hur, B. S. Kong, E. J. Kim, E. W. Shin, and J. S. Chung, *J. Mater. Chem.,* **21**, 11312 (2011).
23. R. J. Smith, M. Lotya, and J. N. Coleman, *New J. Phys*., **12**, 125008 (2010).
24. Z. Peining, A. S. Nair, P. Shengjie, Y. Shengyuan, and S. Ramakrishna, *ACS. Appl. Mater. Interfaces,* **4**, 581 (2012).
25. D. D. Zhang, S. Z. Zu, and B. H. Han, *Carbon*, **47**, 2993 (2009).
26. W. Li, X. Z. Tang, H. B. Zhang, Z. G. Jiang, Z. Z. Yu, X. S. Du, and Y. W. Mai, *Carbon*, **49**, 4724 (2011).
27. N. H. Kim, T. Kuila, and J. H. Lee, *J. Mater. Chem. A,* **1**, 1349 (2013).
28. W. S. Hummers and R. E. Offeman, *J. Am. Chem. Soc.,* **80**, 1339 (1958).
29. B. W. Chieng, N. A. Ibrahim, W. M. Z. W. Yunus, M. Z. Hussein, and V. S. G. Silverajah, *Int. J. Mol. Sci*., **13**, 10920 (2012).
30. C. Bao, L. Song, W. Xing, B. Yuan, C. A. Wilkie, J. Huang, Y. Guo, and Y. Hu, *J. Mater. Chem*., **22**, 6088 (2012).
31. H. Kim and C. W. Macosko, *Macromolecules*, **41**, 3317 (2008).
32. J. Wang, H. Hu, X. Wang, C. Xu, M. Zhang, and X. Shang, *J. Appl. Polym. Sci.*, **122**, 1866 (2011).
33. H. J. Salavagione, G. Martínez, and G. Ellis, *Macromol. Rapid Commun.,* **32**, 1771 (2011).
34. X. Y. Yuan, L. L. Zou, C. C. Liao, and J. W. Dai, *Express. Polym. Lett.,* **6**, 847 (2012).
35. H. B. Zhang, W. G. Zheng, Q. Yan, Z. G. Jiang, and Z. Z. Yu, *Carbon*, **50**, 5117 (2012).
36. M. Wang, W. Wang, T. Liu, and W. D. Zhang, *Compos. Sci. Technol*., **68**, 2498 (2008).
37. K. P. Pramoda, H. Hussain, H. M. Koh, H. R. Tan, and C. B. He, *J. Polym. Sci. Poly. Chem.,* **48**, 4262 (2010).
38. F. Pourfayaz, A. A. Khodadadi, Y. Mortazavi, and H. Jafari, *Plasma Process. Polym.*, **7**, 1001 (2010).
39. W. Zheng and S. C. Wong, *Compos. Sci. Technol.,* **63**, 225 (2003).
40. W. E. Mahmoud, *Eur. Polym. J.,* **47**, 1534 (2011).
41. E. Calahorra, M. Cortazar, and G. M. Guzman, *J. Polym. Sci. Pt. C-Polym. Lett. Ed*., **23**, 257 (1985).
42. P. C. Ma, J. K. Kim, and B. Z. Tang, *Compos. Sci. Technol*., **67**, 2965 (2007).
43. T. Kuila, S. Bose, P. Khanra, N. H. Kim, K. Y. Rhee, and J. H. Lee, *Compos. Pt. A-Appl. Sci. Manuf.*, **42**, 1856 (2011).